Thermomechanical and Optical Properties of Biodegradable Poly(L-lactide)/Silica Nanocomposites by Melt Compounding

Xin Wen,[1,2] Ying Lin,[1,2] Changyu Han,[1] Kunyu Zhang,[1,2] Xianghai Ran,[1,2] Yuesheng Li,[1] Lisong Dong[1]

[1]*State Key Laboratory of Polymer Physics and Chemistry, Changchun Institute of Applied Chemistry, Chinese Academy of Sciences, Changchun 130022, China*
[2]*Graduate School, Chinese Academy of Sciences, Beijing 10080, China*

Received 17 January 2009; accepted 4 June 2009
DOI 10.1002/app.30896
Published online 7 August 2009 in Wiley InterScience (www.interscience.wiley.com).

ABSTRACT: Poly(L-lactide) (PLA)/silica (SiO_2) nanocomposites containing 1, 3, 5, 7, and 10 wt % SiO_2 nanoparticles were prepared by melt compounding in a Haake mixer. The phase morphology, thermomechanical properties, and optical transparency were investigated and compared to those of neat PLA. Scanning electron microscopy results show that the SiO_2 nanoparticles were uniformly distributed in the PLA matrix for filler contents below 5 wt %, whereas some aggregates were detected with further increasing filler concentration. Differential scanning calorimetry analysis revealed that the addition of SiO_2 nanoparticles not only remarkably accelerated the crystallization speed but also largely improved the crystallinity of PLA. An initial increase followed by a decrease with higher filler loadings for the storage modulus and glass-transition temperature were observed according to dynamic mechanical analysis results. Hydrogen bonding interaction involving C=O of PLA with Si—OH of SiO_2 was evidenced by Fourier transform infrared analysis for the first time. From the mechanical tests, we found that the tensile strength and modulus values of the nanocomposites were greatly enhanced by the incorporation of inorganic SiO_2 nanoparticles, and the elongation at break and impact strength were slightly improved. The optical transparency of the nanocomposites was excellent, and it seemed independent of the SiO_2 concentration; this was mainly attributed to the closed refractive indices between the PLA matrix and nanofillers. J Appl Polym Sci 114: 3379–3388, 2009

Key words: nanocomposites; polyesters; silicas; transparency

INTRODUCTION

With increasing environmental awareness around the world, the research and development of biodegradable polymers has attracted more and more attention.[1–3] Poly(L-lactide) (PLA), a typical linear aliphatic thermoplastic polyester, has been viewed as the most popular commercial biodegradable material because it is biodegradable, compostable, and nontoxic to the human body and to the environment; moreover, it can be produced from renewable plant resources (mainly starch and sugar).[4–6] This polymer possesses reasonably good mechanical and optical properties, thermal plasticity, and processability, so it has tremendous market potential for packaging materials, fibers, agricultural films, and biomaterials.[7,8] However, some of its physical properties, such as its toughness, dimensional stability, melt viscosity, crystallization rate, and gas barrier properties, are still not satisfactory for processing and application. Consequently, there is a sustained interest in overcoming these disadvantages without a drastic loss in its general performance to meet various end-use applications.

Over the last few years, a new class of mineral-reinforced thermoplastics known as *nanocomposites* has attracted increasing interest for researchers in the field of polymer and materials science from both academia and industry.[9–11] Fillers as dispersed phases in nanocomposites are nanometer sized, preferably with at least one of its dimensions on the order of a few nanometers (1–100 nm). Because of the small particle size and extremely high surface area, the incorporation of nanoparticles into a polymer creates a great amount of interphase and changes the intermolecular interaction of the matrix. As a result, dramatic improvements in the physical and mechanical properties, including stiffness and toughness, thermal stability, gas barrier properties, and electrical and thermal conductivity, can be achieved by the incorporation of a few weight percentages of particulate fillers into polymer matrices.

On the basis of these advantages of nanocomposites, many excellent studies have been reported on

Correspondence to: L. Dong (dongls@ciac.jl.cn).
Contract grant sponsor: Chinese Academy of Science Direction Project; contract grant number: KTCX-YW-208.

the preparation and properties of PLA nanocomposites. PLA/layered silicate nanocomposites have been extensively studied, including some reviews.[12–14] PLA nanocomposites incorporating hydroxyapatite, carbon nanotubes, calcium carbonate, and titanium dioxide have also been reported.[15–18] The crystallinity, thermal stability and mechanical, gas-barrier, degradation, and flame-retardant properties of PLA have been greatly improved. Unfortunately, some original properties, such as optical transparency, were lost in these prepared nanocomposites.

Fumed silica (SiO_2) has also been widely used as a nanofiller the preparation of polymer/SiO_2 nanocomposites.[19–21] It possesses advantages of a light mass, low price, rich resource, high strength and modulus, and good thermal stability; more importantly, it has almost the same refractive index as PLA, so it is believed that the outstanding properties are obtained by the preparation of PLA/SiO_2 nanocomposites. To this point, few studies on PLA/SiO_2 nanocomposites have been reported. Yan et al.[22] prepared PLA/SiO_2 nanocomposites via two steps: the grafting of L-lactic acid oligomer onto the surface of SiO_2 followed melt blending with PLA. The resulting nanocomposites had improved mechanical properties. Subsequently, the same research group,[23] in another study, successfully synthesized plasticized PLA/SiO_2 nanocomposite materials by a sol–gel process. Recently, Wu et al.[24] prepared PLA/SiO_2 nanocomposites (PLASNs) by the *in situ* melt polycondensation of L-lactic acid in the presence of acidic SiO_2 sol and improved the dispersion of SiO_2 nanoparticles in the final nanocomposites. These methods were positive in improving the performance of PLA, but they often resulted in extra cost and the use of a toxic organic solvent, which is undesired with regard to environmental concerns.

When one considers the processing technology and cost for preparing PLASNs, direct melt compounding based on commercial raw materials is a more applicable and economical compared with solution blending, sol–gel processes, and so on. To the best of our knowledge, no detailed investigation on PLASNs has been reported hitherto by this convenient method. In this study, PLASNs were prepared by melt compounding in a Haake (Karlsruhe, Germany) mixer. The interaction between PLA and SiO_2 was studied by Fourier transform infrared (FTIR) spectroscopy. The effects of SiO_2 loading on the phase morphology, microstructure, and thermal and mechanical properties of the nanocomposites were studied through scanning electron microscopy (SEM), differential scanning calorimetry (DSC), dynamic mechanical analysis (DMA), and mechanical tests. In addition, the dependence of the optical transparency on the SiO_2 content for the nanocomposites was also investigated.

EXPERIMENTAL

Materials

The PLA (4032D) used in this study was a commercial product of Natureworks Co., Ltd. (USA), and had a high optical purity of about 98% L-lactide content. It exhibited a density of 1.24 g/cm^3, a weight-average molecular weight of 250 kDa, a polydispersity of 1.70 (gel permeation chromatography analysis), and a glass-transition temperature (T_g) and melting temperature (T_m) of 60.48 and 166.40°C (DSC analysis), respectively.

The nanosilica (Aerosil 200) was supplied by Degussa AG (Hanau, Germany). It was hydrophilic pyrogenic SiO_2 with a specific surface area of 200 m^2/g (>99.8% SiO_2). The SiO_2 nanoparticles were aggregates and had an average primary particle size of 12 nm.

Preparation of the nanocomposites

PLA was mechanically mixed with nanosilica from 1 to 10 wt %. Before blending, PLA and nanosilica were dried *in vacuo* at 90 and 110°C for 24 h, respectively. Melt blends were prepared with a Haake batch intensive mixer (Haake Rheomix 600) with a batch volume of 50 mL. The components were mixed at a screw speed of 60 rpm for 5 min at 175°C. The torque was continuously monitored during the whole mixing process. Also, the neat PLA was subjected to the mixing treatment to create the same thermal history as that of the blends. After mixing, all of the compounds were cut into small pieces. Then, all of samples were compression-molded into sheets with thicknesses of 1.0 and 4.0 mm at 180°C for various tests. For convenience, the PLASNs are denoted as PLASNx in the following discussion, where x represents the weight percentage of SiO_2 nanoparticles.

Characterization

The morphologies of the fracture surfaces of the neat PLA and PLASNs were examined with an XL30 environmental scanning electron microscope with a field-emission gun (FEI Co., Eindhoven, The Netherlands). The samples were frozen well in liquid nitrogen and quickly broken off to obtain a random brittle-fractured surface. A layer of gold was sputter-coated uniformly over all of the fractured surfaces before SEM observations.

The thermal parameters of the PLA and PLASNs were measured by a DSC-7 (PerkinElmer, Waltham, MA) under a nitrogen flow. All samples were heated from 30 to 200°C at a heating rate of 50°C/min and kept isothermal for 3 min to erase the previous thermal history. Then, they were cooled to 0°C at 50°C/

min, and subsequently, the second scan as result curves was performed between 0 and 200°C at a heating rate of 10°C/min. The T_g originated from the midpoint of the transition. Both the cold crystallization temperature (T_{cc}) and T_m were determined from the peak temperature.

DMA was carried out with a Diamond DMA dynamic mechanical analyzer (PerkinElmer, American) in the tensile mode. The samples ($20 \times 6 \times 1$ mm^3) were measured over a wide temperature range of −30 to 140°C at a heating rate of 3°C/min and at a frequency of 1 Hz. The viscoelastic properties, such as the storage modulus (E') and mechanical loss factor ($\tan \delta = E''/E'$, where E'' is the loss modulus), were recorded as a function of the temperature.

Infrared (IR) spectroscopy measurements were recorded with a Bruker (Ettlingen, Germany) Vertex 70 FTIR spectrophotometer, and 64 scans were collected with a spectral resolution of 1 cm^{-1}. The tetrahydrofuran solution (1 mg/mL) containing the blend samples were cast onto a conventional KBr disk, allowed to evaporate at room temperature, and vacuum-dried at 50°C for 24 h. Subsequently, all KBr disks containing samples were kept isothermal *in vacuo* at 200°C for 5 min to erase the previous history, then quickly taken out, and quenched to room temperature for FTIR measurement. The SiO_2 particles were mixed with KBr grains at a weight ratio of 0.5–1% and then compressed into a thin disk for the testing.

Uniaxial tensile tests were performed with an Instron 1121 testing machine (Canton, MA). Specimens ($20 \times 4 \times 1$ mm^3) were cut from the previously compression-molded sheet into a dumbbell shape. The measurements were conducted at a crosshead speed of 5 mm/min at room temperature. The V-notched specimens ($55 \times 6 \times 4$ mm^3) were tested to measure the impact strength according to GB1843-93 procedures with an impact testing machine (CEAST, Chengde, China). All tests were carried out at room temperature and 50% relative humidity. At least five runs for each sample were measured, and the results were averaged.

The light transmittance and haze values of the pure PLA and PLASN sheets were measured with a photoelectric haze instrument (WGW, Suzgou, China) at room temperature. The sheets were prepared by melting and then quick quenching with a thickness of 1.00 ± 0.02 mm.

RESULTS AND DISCUSSION

Structure and morphology

It is well known that the properties of nanocomposites are highly dependent on the filler dispersion and adhesion with the polymer matrix. Figure 1(a) shows the SEM image of the pure PLA fracture surface, which was smooth and featureless. As for the PLASNs, the SiO_2 particles were detected as white dots. They were spherical in shape, and the diameter was dependent on the amount of SiO_2. When the SiO_2 content was less than 5 wt % [Fig. 1(b–d)], the nanoparticles were uniformly distributed in the PLA matrix. They exhibited many monodisperse particles and only a few aggregates integrated with three to five particles. The aggregates did not exceed 100 nm in diameter. However, larger aggregates were found, and the size of aggregates increased substantially in these micrographs with higher SiO_2 loadings [Fig. 1(e,f)]. At the highest SiO_2 content (10 wt %), particle sizes ranging from 120 to 750 nm were detected. These results are in good agreement with the findings of Wu et al.[25] and Bikiaris et al.,[26] who reported that increasing the content of SiO_2 led to large aggregates. It was hard to break aggregates as completely single particles during compounding when the nanoparticle content was too high because a strong interaction still existed among the nanoparticles.

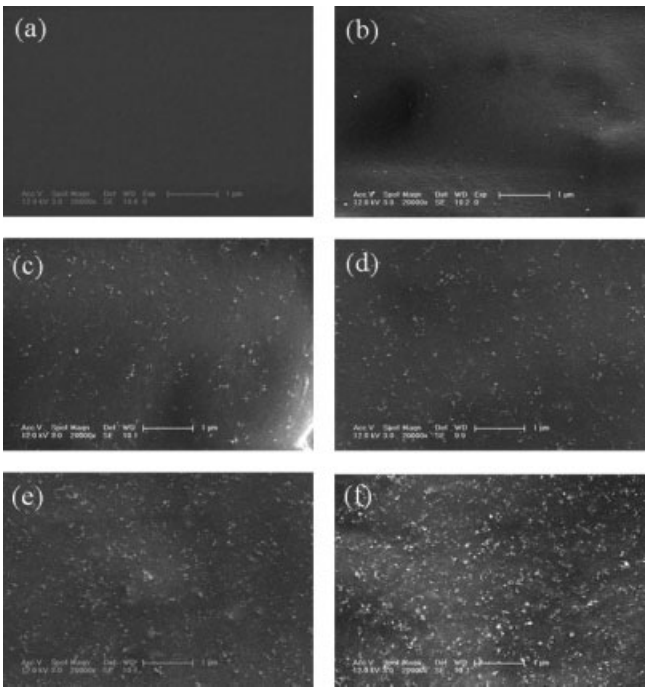

Figure 1 SEM micrographs of the fractured surfaces of the PLA and PLASNs: (a) pure PLA, (b) PLASN1, (c) PLASN3, (d) PLASN5, (e) PLASN7, and (f) PLASN10.

Thermal and crystallization behavior

The physical properties of the nanocomposites could be significantly affected by the crystallization characteristics of PLA. Figure 2 shows the second heating scans of the DSC thermograms of the neat PLA and PLASNs with various filler loadings, and Table I summarizes the results obtained from this heating run for all of the samples. The measurements were

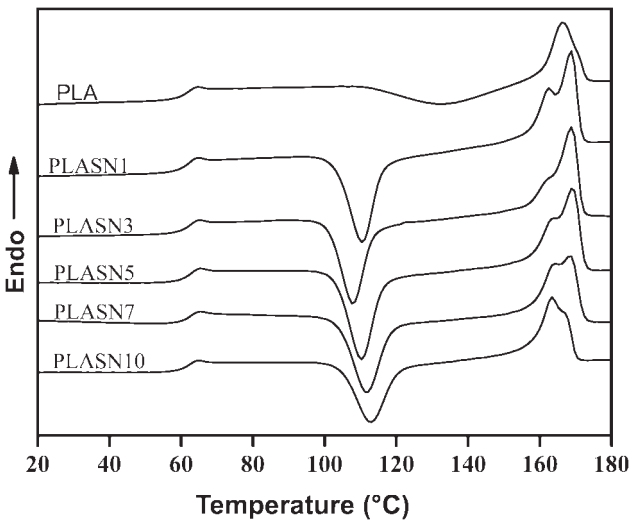

Figure 2 Second-heating DSC curves of the PLA and PLASNs at a heating rate of 10°C/min.

performed immediately after the melt-quenching scans, so the samples had the same thermal history without an aging cycle. The curves revealed the following thermal events with increasing temperature: the glass–rubber transition (characterized by T_g), cold crystallization process [characterized by T_{cc} and the cold crystallization enthalpy (ΔH_{cc})], and the melting process with two components (characterized by T_{m1}, ΔH_{m1}, T_{m2}, and ΔH_{m2}, where ΔH_m is the melting enthalpy). Comparing the thermograms and calorimetric parameters collected in Table I, one can see that with a filling of SiO_2, T_g was almost unchanged; only small differences existed within 1°C. It seemed that the chain segment mobility of the PLA phase was not influenced by the introduction of SiO_2 nanoparticles. With regard to the limitations of the DSC technique, more discussions on this topic are presented with the DMA results.

As shown in Figure 2, neat PLA represented a tiny broad exothermic peak at 133°C, which indicated a rather low cold crystallization capability. However, in the case of PLASNs, this peak was sharper and appeared at much lower temperature, and the crystallization enthalpies increased correspondingly (Table I). These results suggested that the incorporation of SiO_2 enhanced the cold crystalline ability of PLA. The significant decrease in T_{cc} was ascribed to a nucleating effect of the filler, which accelerated the crystallization speed of PLA. The concentration dependence of the nucleating effect was also observed in similar compositions of PLA/clay nanocomposites.[27] By careful analysis, it was easy to detect that T_{cc} decreased to the lowest 107.80°C with 3 wt % loadings. When the content of SiO_2 continued to increase, T_{cc} followed and shifted to the higher temperature. This result can be explained by the agglomeration of the nanoparticles. More nanoparticles were added, and more aggregates were formed. In general, larger aggregates contributed to the crystallization of PLA. This significantly conformed by the gradually decrease of ΔH_{cc} that corresponded to the increase in filler content. In other words, when these nanoparticles were well dispersed in the PLA matrix, the number of them was very large, even at a filler content of 1 wt %, which was enough to form the nucleating sites and promote the growth of PLA crystals.

In parallel with the shift in T_{cc}, the T_m of PLA component also gradually shifted down with increasing SiO_2 content. Interestingly, the melting peak had a transition from a single peak to two separate peaks. A similar phenomenon with the bimodal melting peaks was also reported for other PLA blends.[28] It was induced during the slow DSC scans when the less perfect crystals had enough time to melt and reorganize into crystals with higher structural perfection and remelt at higher temperature. By considering the theoretical enthalpy of completely crystalline PLA (ΔH_m^*) as 93.1 J/g,[29] we estimated the value of crystalline degree (χ_c) of PLA in different systems. χ_c of the composites was based on the following equation:

$$\chi_c = \frac{\Delta H_m}{(1-\phi)\Delta H_m^*} \times 100\%$$

where ϕ is the weight fraction of the filler in the nanocomposite and ΔH_m is the melting enthalpy (J/g) that was calculated from the fusion peak in

TABLE I
Thermal and Crystalline Properties of the PLA and PLASNs

Sample	T_g (°C)	T_{cc} (°C)	T_{m1} (°C)	T_{m2} (°C)	ΔH_{cc} (J/g)	ΔH_m (J/g)	Crystallinity (%)
PLA	60.48	133.30		166.40	21.27	23.98	25.76
PLASN1	60.71	110.46	162.50	168.61	34.32	37.21	40.37
PLASN3	61.10	107.87	162.60	168.70	32.42	34.57	38.28
PLASN5	61.22	110.26	163.40	169.05	32.25	32.16	36.36
PLASN7	60.68	111.72	164.12	168.38	30.99	29.20	33.72
PLASN10	60.56	112.88	163.44	166.91	28.64	27.41	32.71

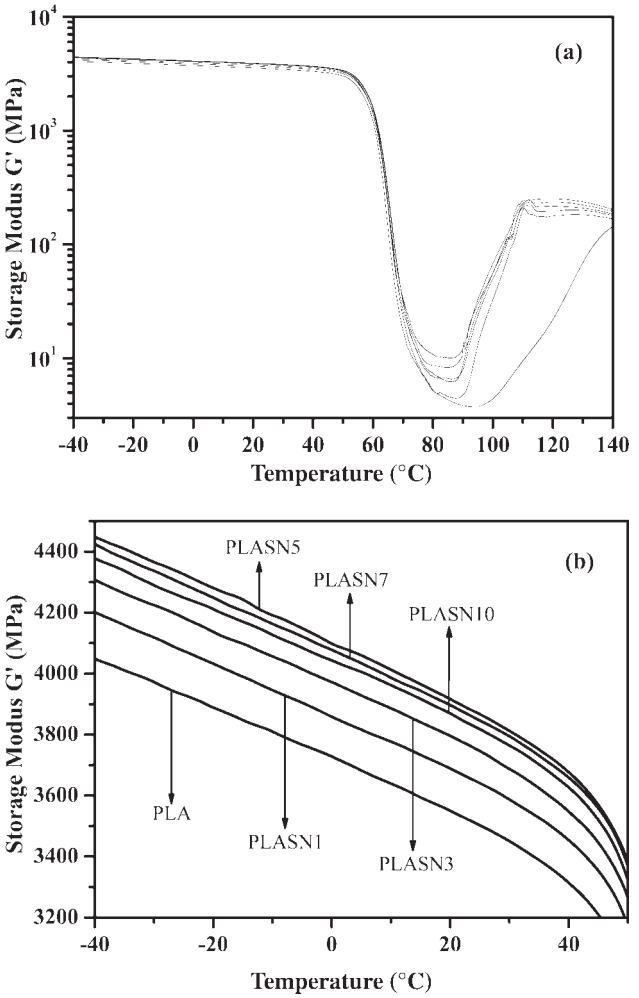

Figure 3 Effect of the SiO_2 concentration on the storage modulus (G') of the PLASNs: (a) −40 to 140°C and (b) −40 to 50°C.

DSC curve. According to the data listed in Table I, the χ_c values of all of the nanocomposites were greatly increased compared to that of neat PLA. In the meantime, χ_c gradually decreased with increasing content of SiO_2. This phenomenon has been reported in many other articles.[30,31] Generally, with the addition of lower contents of nanoparticles, the polymer in the nanocomposite, especially PLA, formed crystals much more easily because of the nucleation effect of the nanoparticles. However, when it achieved a certain content, the appearance of some aggregates restricted the crystallization behavior of PLA.

DMA

DMA was used to evaluate the effect of the SiO_2 nanoparticles on the thermomechanical properties of the PLA matrix because of its sensitivity to the relaxation behavior of the materials examined. The mechanical relaxation data of the composites with

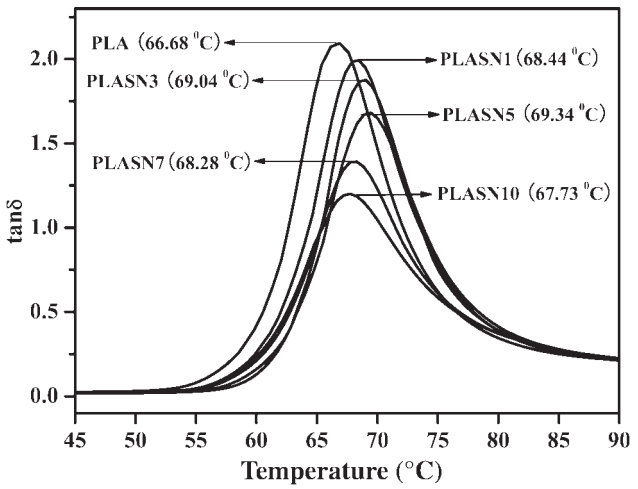

Figure 4 Effect of the SiO_2 concentration on the tan δ of the PLASNs.

different contents of SiO_2 are depicted later in Figures 4 and 5 in the form of E' and tan δ, respectively.

Figure 3(a) shows the variations of E' as a function of temperature for the PLA and PLASNs. For all of the samples, the following characteristic E' changes with increasing temperature were observed: a gradual decrease in the region of −40 to 50°C, a rapid drop below 55–70°C due to the glass–rubber transition (T_g), an increase in the cold crystallization range (ca. 110°C) due to reinforcement by the crystallites being formed, and then, a decrease as a result of the premelting process. Comparing the E' values of the different samples below T_g, as magnified in Figure 3(b), we realized that all of nanocomposites had higher E' values than did the initial PLA. A substantial increase in E' was recorded with increasing SiO_2 content up to 5 wt %, where the maximum value was reached. This behavior was attributed to the tendency of SiO_2 to form aggregates at higher concentrations, as already proven by the SEM study.

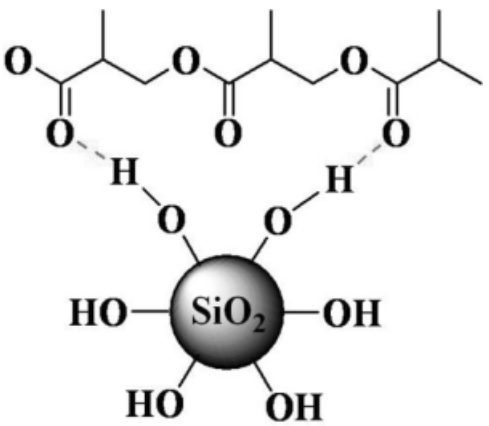

Figure 5 Schematic illustration of the hydrogen-bonding interactions between the PLA and SiO_2.

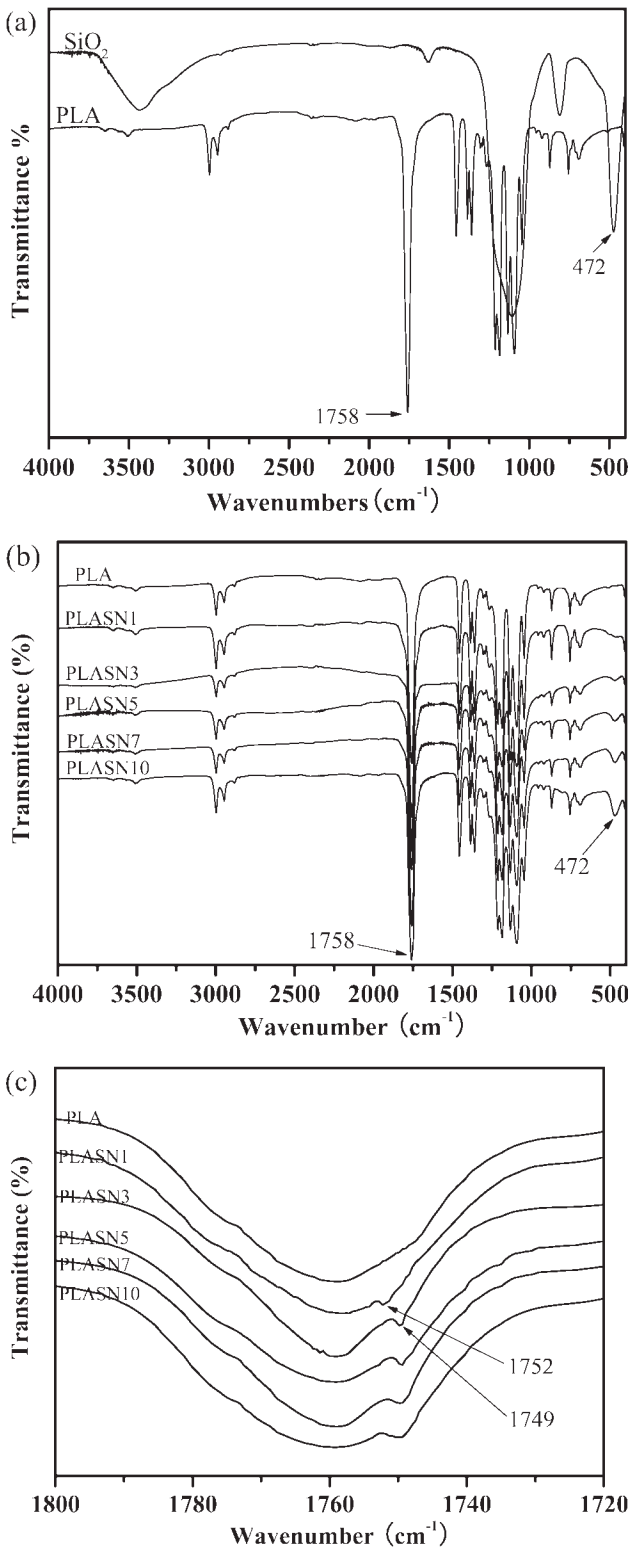

Figure 6 FTIR spectra of the pure PLA and PLASNs: (a) pure PLA and SiO_2 nanoparticles and (b) pure PLA and PLASNs and (c) magnified FTIR spectra between 1800 and 1720 cm^{-1}.

Similar relationships were reported in PP/SiO_2 nanocomposites by Bikiaris et al.[32] It was obvious that E' of the PLASNs increased dramatically in the cold crystallization range as compared with the pure PLA, which suggested that the incorporation of SiO_2 enhanced the cold crystalline ability of PLA because of the nucleation effect. This was in good agreement with the DSC results discussed previously.

Figure 4 shows the variation of tan δ with temperature for the PLA and PLASNs. The results indicate that tan δ slightly increased for filler contents up to 5 wt % but decreased gradually with further increases in SiO_2 concentration. This was different not only from the previous work on PI/SiO_2 nanocomposites,[33] in which T_g increased as a function of filler loading, but also from the result for epoxy resin/SiO_2 nanocomposites,[34] which showed a sharp T_g depression. In many cases, the dispersion and surface conditions of the nanoparticles have played important roles in the changes in T_g. Molecular dynamic simulations of polymer melts in the presence of nanoparticles have shown that the dynamics of the polymer melts can be influenced by polymer–nanoparticle interactions.[35] Here, *dynamics* means the mobility of the polymer chains. Strongly attractive polymer–nanoparticle interactions slow the dynamics with respect to those of a pure polymer melt, whereas nonattractive interactions enhance the dynamics. Macroscopically, a change in the dynamics results in a shift in T_g. In this study, SiO_2 nanoparticles possessed lots of Si—OH groups on the surfaces, and PLA had C=O groups in its chains, so molecular interaction, that is, hydrogen bonding may have existed between them. A schematic illustration of the interaction is described in Figure 5.

FTIR analysis of hydrogen bonding

The FTIR technique is sensitive enough to verify hydrogen-bonding formation in various systems.[36–38] Particularly, because the C=O stretching vibration intensity of PLA is excessively strong, its peak often goes beyond the full scale if the testing film is somewhat thick. To obtain a film with a suitable thickness for FTIR measurement, a new method, as reported in our previous article,[38] dissolves the melt-compounding composites and then recasts them onto KBr disks. The IR spectra of the pure PLA and SiO_2 nanoparticles are presented in Figure 6(a). From the curve of PLA, we observed that there was a strong absorption band at 1758 cm^{-1}, which corresponded to the C=O stretching vibration. Additionally, the band at 2997 cm^{-1} was assigned to the C—H stretching vibrations of CH_3 groups in the side chains, and the band 2946 cm^{-1} was attributed to the —CH— in the stem chains of PLA. Similarly, peaks at the wave numbers 1109, 809, and 472 cm^{-1} were caused by the bending vibration of the functional group Si—O, as shown in the curve of SiO_2. The peak at 3432 cm^{-1} represents the stretching vibration of the

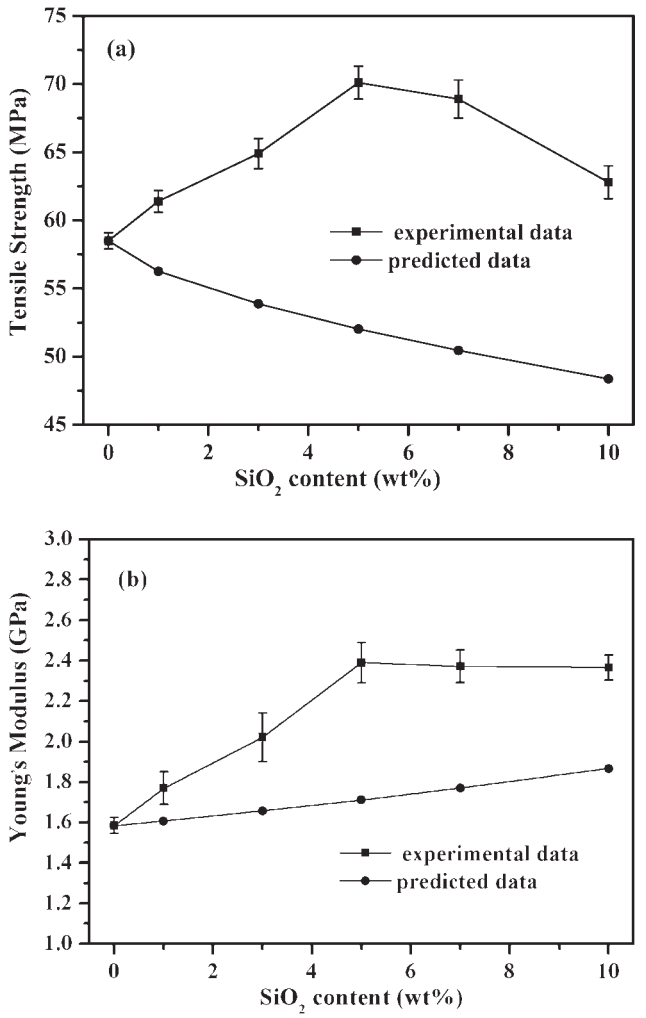

Figure 7 Variation of the (a) tensile strength and (b) Young's modulus of the nanocomposites with the nanoparticle loading.

functional group —OH. It was obvious that the strongest peak of SiO_2 at 1109 cm^{-1} overlapped with the peak at 1093 cm^{-1}, which corresponded to the —C—O— stretching vibration of PLA, so the second strongest peak at 472 cm^{-1} was selected to quantify SiO_2 in the PLASNs.

Figure 6(b) shows the IR spectra of the PLASNs, and the curve of pure PLA is presented again for comparison. It was apparent that pure PLA had no absorption at 472 cm^{-1}. However, as the SiO_2 content gradually increased, the intensity at 472 cm^{-1} for the PLASNs became stronger and stronger accordingly. To investigate the changes of C=O, the curves between 1800 and 1720 cm^{-1} were magnified, as shown in Figure 5(c). Interestingly, the stretching vibrations of C=O for the PLASNs were all split up into two peaks. One peak at 1758 cm^{-1} was assigned to the original C=O vibration of PLA; the other blueshifted to a lower wave number, which was ascribed to the interaction of PLA and SiO_2. This indicated that hydrogen-bonding interaction existed between the Si—OH and the C=O of PLA. By comparing the position and intensity of these peaks, we determined that the interaction between them was drastically dependent on the content and dispersion of SiO_2, which was in accordance with previous SEM results.

On the basis of the hydrogen bonding formation, the changes in T_g for the PLASNs could be easily interpreted. Because of the hydrogen-bonding interaction, which slowed the dynamics of the PLA chains, there existed less free volume at the SiO_2–PLA interface, and T_g shifted to a higher temperature within 5 wt % of SiO_2 loading. As the filler loading increased beyond 5 wt %, the appearance of some aggregates weakened the interaction because of the decreased interphase, and the previously enhanced dynamics decreased to a certain extent and resulted in a lower T_g. Overall, the hydrogen-bonding interaction between PLA and SiO_2 was not strong enough, so the changes in T_g seemed to be indistinctive in the DSC data. However, the differences in T_g in the PLASNs were easily detected by DMA testing because of its higher sensitivity to T_g.

Mechanical properties

The mechanical properties were measured to evaluate the reinforcing effect of the nanoparticles on PLA. Because of the very high surface area of the nanoparticles in the nanocomposites, the applied stresses were expected to be easily transferred from the matrix onto the SiO_2 particles and to result in an enhancement in the mechanical properties. The results of tension testing were calculated and are plotted in Figure 6. Meanwhile, for comparison, the Young's modulus and tensile strength of the composites were predicted, respectively, by Guth's equation[39]:

$$E_c = E_m\left(1 + 2.5\phi_f + 14.1\phi_f^2\right) \quad (1)$$

and Nicolais–Narkis theory[40]:

$$\sigma_{yc} = \sigma_{ym}\left(1 - 1.21\phi_f^{2/3}\right) \quad (2)$$

where E and σ_y are the Young's modulus and tensile strength, respectively; the subscripts m and c denote the composite and the matrix, respectively; and ϕ_f is the volume fraction of particles, which can be calculated with eq. (3):

$$\phi = \rho_m W_f/[(\rho_m - \rho_c)W_f + \rho_c] \quad (3)$$

where W_f is the weight fraction of particles and ρ_m and ρ_c are the densities of the PLA matrix (1.24 g/m^3) and SiO_2 nanoparticles (2.20 g/m^3), respectively.

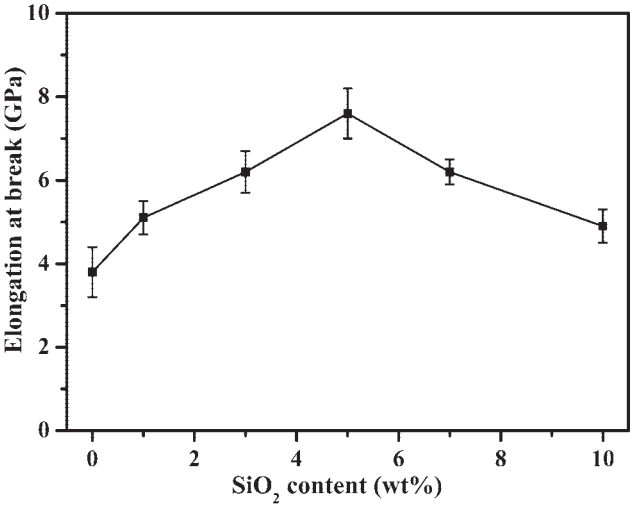

Figure 8 Variation of the elongation at break of the nanocomposites with the nanoparticle loading.

Figure 7(a) shows a comparison of the predicted tensile strength with the measured values in the studied nanocomposites. Clearly, the predicted values continuously decreased with increasing amount of SiO_2. However, the experimental values in all of composites were higher than the theoretical values. Even with 10 wt % SiO_2, in which a slight drop was also observed in the experimental value, the experimental value was still higher than the theoretical value. These results were attributed to the limitations of Guth's equation, which is only suitable for those systems with poor adhesion between the particles and the matrix, but in this system, there existed some interaction between SiO_2 and PLA, as discussed previously. Furthermore, as can be seen in the diagrams, the measured values were greatly affected by the SiO_2 content. The tensile strength gradually increased for SiO_2 content up to 5 wt % and then decreased slowly with further increases in the filler loading. PLASN5 exhibited the highest tensile strength (70 MPa), which improved nearly 20% compared to that of neat PLA. As reported in many results, the particle size had a significant effect on the strength of the particulate-filled polymer composites, which generally decreases with increasing size. When the loading increased beyond 5 wt %, more and more aggregates formed, and their size increased, which resulted in a gradual decrease in the tensile strength of the composites. These results are also in good agreement with the previously discussed results from the SEM images.

The Young's modulus values of the nanocomposites are shown in Figure 7(b). From the predicted results, the addition of rigid particles into the PLA matrix easily improved the modulus values because the rigidity of inorganic fillers is generally much higher than that of organic polymers. However, there were some different features for the trends of the measured modulus values. The moduli increased gradually for SiO_2 contents up to 5 wt % and then remained at almost the same level with further increases in filler loading. Fu et al.[41] indicated that there was a critical particle size, above which there was no effect on the composites modulus, but the effect was significant when the particle size was below it. In this study, the average particle size corresponding to a 5 wt % concentration was the possible critical size. Consequently, the modulus increased significantly with less than 5 wt % SiO_2, but it was insensitive to higher concentration. Meanwhile, it was clear that with the same SiO_2 content, each of the measured moduli of the nanocomposites was much higher than that of the predicted value. This was attributed to the effect of the hydrogen-bonding interaction between PLA and SiO_2, as discussed previously. In addition, the measured modulus was also dependent on the crystallinity of PLA. According to the previously discussed DSC results, the crystallinity of PLA was markedly improved by the incorporation of the SiO_2 nanoparticles, so the modulus values of the PLASNs increased remarkably and were much larger than the predicted values.

Generally, the toughness of polymer materials should be determined by the area under a stress–strain curve, but it is usually estimated by the elongation at break if the tensile strength does not change a lot. To characterize the effect of SiO_2 on the toughness of the nanocomposites, Figure 8 plots the elongation at break of the nanocomposites as a function of SiO_2 content. The elongation at break increased only a little in the PLASNs, so it seems that there was an insensitive effect on the toughness with the introduction of SiO_2 into the PLA matrix.

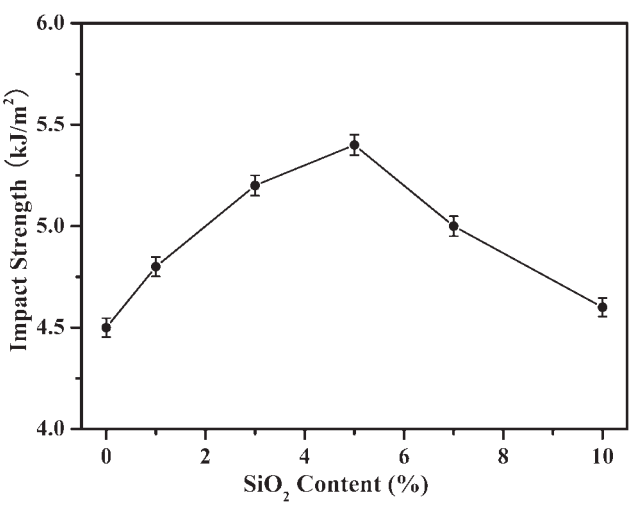

Figure 9 Variation of the notched impact strength of the nanocomposites with the nanoparticle loading.

Another characteristic parameter of the toughness of a polymer material is its notched impact strength. The notched impact strengths for the PLA and PLASNs are shown in Figure 9. Similarly, the SiO_2 loadings had a slight effect on the improvement of the matrix toughness. Similar results were also obtained for other nanocomposites systems.[19] Zhang et al.[42] demonstrated that the keys to toughening nonlayered nanoparticles/polymer composites included sufficient mobility of nanoparticles in the polymer matrix, low particle–particle attraction, and strong filler–matrix interaction. However, our experiments were carried out at room temperature, which was far below the T_g of PLA. As a result, the effect of nanosilica on the toughness of PLA was indistinct.

Optical properties

PLA is one of a few transparent biodegradable polymers in commercial products. Undoubtedly, it is advantageous for food packing materials and other consumer products, but most PLA-based nanocomposites have lost essential characteristics because of the different refractive indices between the PLA matrix and nanofillers. The refractive index of the SiO_2 nanoparticles chosen in this study was 1.46, which was very close to that of the PLA matrix, which had a value of 1.45.

The visible light transmittance and haze value of the neat PLA and PLASNs are plotted in Figure 10. It was obvious that the transmittance fluctuated at 85% and seemed independent on the SiO_2 concentration. Correspondingly, the haze value of all of the samples varied near 5 and were almost unaffected by the filler loadings.

To further study the effect of the SiO_2 particles on the transparency of the nanocomposites, the photographs of the PLA and PLASN sheets covered on the same graphic pattern and collected by a digital camera were shown in Figure 11. It was apparent that each sheet possessed excellent transparency, and the letters below it were clearly observed, even in the PLASN10 with the highest SiO_2 content. This result was consistent with those from the previous discussion. It indicates that the transparency of the PLASNs was mainly due to almost the same refractive index of the two components and was little affected by the filler loadings and their dispersion in the matrix.

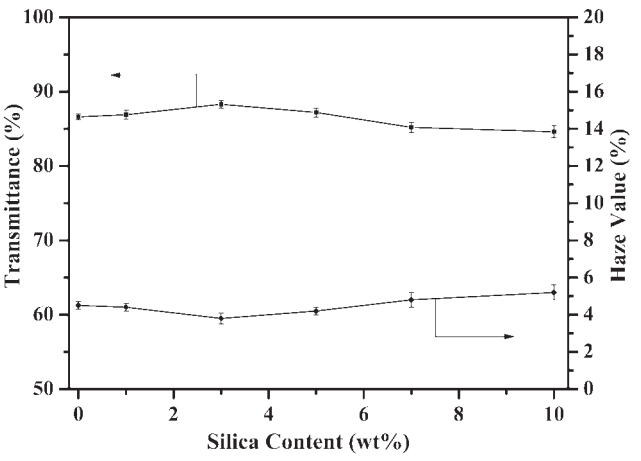

Figure 10 Effect of the SiO_2 concentration on the transparency and haze for the PLASNs.

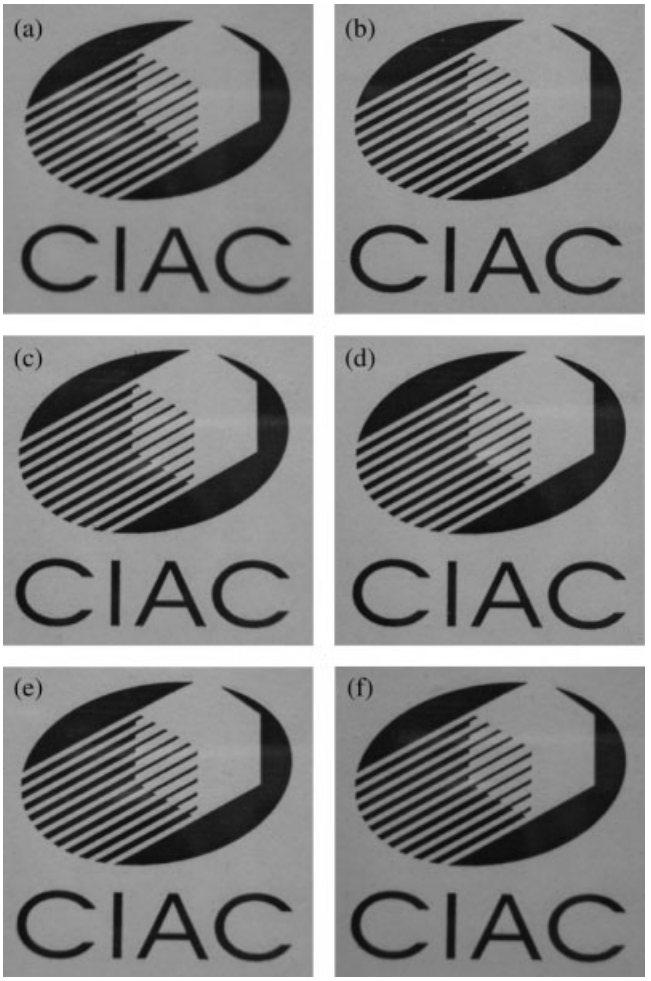

Figure 11 Photographs of the PLA and PLASN sheets on a graphic pattern: (a) pure PLA, (b) PLASN1, (c) PLASN3, (d) PLASN5, (e) PLASN7, and (f) PLASN10.

CONCLUSIONS

PLA/SiO_2 binary nanocomposites were prepared by melt compounding to investigate the effects of nanofiller loadings on the phase morphology, thermomechanical properties, and optical transparency of the nanocomposites. A good dispersion of the SiO_2 nanoparticles in PLA was achieved for filler contents below 5 wt %, but some aggregates were found with

higher concentrations. The addition of SiO_2 nanoparticles remarkably enhanced the cold crystallization ability and largely improved the crystallinity of PLA. The DMA results show that T_g of PLA slightly shifted to a higher temperature because of the weak interaction between the PLA and SiO_2 nanoparticles. The FTIR results indicate that hydrogen-bonding interaction between the C=O group of PLA and the surface Si—OH group of SiO_2 existed in the PLASNs. The tensile strength and modulus of the nanocomposites were significant enhanced by the introduction of stiff nanoparticles, but the elongation at break and the impact strength were not much affected by the presence of SiO_2 nanoparticles. Nanocomposites with a high transparency, similar to that of pure PLA, were obtained without dependence on the amount of SiO_2 nanoparticles; this was attributed to the close refractive indices of the two components.

References

1. Bhattacharya, M. Polym Eng Sci 2005, 45, 1452.
2. Yu, L.; Dean, K.; Li, L. Prog Polym Sci 2006, 31, 576.
3. Dong, T.; Kai, W.; Pan, P.; Cao, A.; Inoue, Y. Macromolecules 2007, 40, 7244.
4. Garlotta, D. J Polym Environ 2001, 9, 63.
5. Lunt, J. Polym Degrad Stab 1998, 59, 145.
6. Hakkarainen, M. Adv Polym Sci 2002, 157, 113.
7. Sodergard, A.; Stolt, M. Prog Polym Sci 2002, 27, 1123.
8. Lim, L.-T.; Auras, R.; Rubino, M. Prog Polym Sci 2008, 33, 820.
9. Alfred, J.; Crosby, L. J. Polym Rev 2007, 47, 217.
10. Fedullo, N.; Sorlier, E.; Sclavons, M.; Bailly, C.; Lefebvre, J.; Devaux, J. Prog Org Coat 2007, 58, 87.
11. Tjong, S. C. Mater Sci Eng R 2006, 53, 73.
12. Maiti, P.; Yamada, K.; Okamoto, M.; Ueda, K.; Okamoto, K. Chem Mater 2002, 14, 4654.
13. Ray, S. S.; Okamoto, M. Prog Polym Sci 2003, 28, 1539.
14. Ray, S. S.; Bousmina, M. Prog Mater Sci 2005, 50, 962.
15. Qiu, X.; Hong, Z.; Hu, J.; Chen, L.; Chen, X.; Jing, X. Biomacromolecules 2005, 6, 1193.
16. Chen, G.; Kim, H.; Park, B.; Yoon, J. Macromol Chem Phys 2007, 208, 389.
17. Kim, H. S.; Park, B. H.; Choi, J. H.; Yoon, J. S. J Appl Polym Sci 2008, 109, 3087.
18. Tsuji, H.; Kawashima, Y.; Takikawa, H.; Tanaka, S. Polymer 2007, 48, 4213.
19. Bikiaris, D. N.; Papageorgiou, G. Z.; Pavlidou, E.; Vouroutzis, N.; Palatzoglou, P.; Karayannidis, G. P. J Appl Polym Sci 2006, 100, 2684.
20. Ruan, W. H.; Huang, X. B.; Wang, X. H.; Rong, M. Z.; Zhang, M. Q. Macromol Rapid Commun 2006, 27, 581.
21. Zou, H.; Wu, S.; Shen, J. Chem Rev 2008, 108, 3893.
22. Yan, S.; Yin, J.; Yang, Y.; Dai, Z.; Ma, J.; Chen, X. Polymer 2007, 48, 1688.
23. Yan, S.; Yin, J.; Yang, J.; Chen, X. Mater Lett 2007, 61, 2683.
24. Wu, L.; Cao, D.; Huang, Y.; Li, B. Polymer 2008, 49, 742.
25. Wu, C.; Zhang, M.; Rong, M.; Friedrich, K. Compos Sci Technol 2002, 62, 1327.
26. Bikiaris, D. N.; Vassiliou, A.; Pavlidou, E.; Karayannidis, P. Eur Polym J 2005, 41, 1965.
27. Di, Y. W.; Iannace, S.; Di, M. E.; Nicolais, L. J Polym Sci Part B: Polym Phys 2005, 43, 689.
28. Zhang, L. L.; Xiong, C. D.; Deng, X. M. Polymer 1996, 37, 235.
29. Aslan, S.; Calandrelli, L.; Laurienzo, P.; Malinconico, M.; Migliaresi, C. J Mater Sci 2000, 35, 1615.
30. Nam, P. H.; Okamoto, M.; Kotaka, T.; Hasegawa, N.; Usuki, A. Polymer 2001, 42, 9633.
31. Sinha, R. S.; Maiti, P.; Okamoto, M.; Yamada, K.; Ueda, K. Macromolecules 2002, 35, 3104.
32. Vladimirov, V.; Betchev, C.; Vassiliou, A.; Papageorgiou, G.; Bikiaris, D. Compos Sci Technol 2006, 66, 2935.
33. Shang, X. Y.; Zhu, Z. K.; Yin, J.; Ma, X. D. Chem Mater 2002, 14, 71.
34. Sun, Y. Y.; Zhang, Z. Q.; Moon, K. S.; Wong, C. P. J Polym Sci Part B: Polym Phys 2004, 42, 3849.
35. Glotzer, S. C.; Paul, W. Annu Rev Mater Res 2002, 32, 401.
36. Mikhaylova, Y.; Adam, G.; Häussler, L.; Eichhorn, K. J.; Voit, B. J Mol Struct 2006, 788, 80.
37. Zhou, S.; Zheng, X.; Yu, X.; Wang, J.; Weng, J.; Li, X.; Feng, B.; Yin, M. Chem Mater 2007, 19, 247.
38. Lin, Y.; Zhang, K. Y.; Dong, Z. M.; Dong, L. S.; Li, Y. S. Macromolecules 2007, 40, 6257.
39. Guth, E. J Appl Phys 1945, 16, 20.
40. Nicolais, L.; Narkis, M. Polym Eng Sci 1971, 11, 194.
41. Fu, S.; Feng, X.; Lauke, B.; Mai, Y. Compos B 2008, 39, 933.
42. Zhou, T.; Ruan, W.; Rong, M.; Zhang, M.; Mai, Y. Adv Mater 2007, 19, 2667.